Evidence of cathodic peroxydisulfate activation via electrochemical reduction at Fe(II) sites of magnetite-decorated porous carbon: Application to dye degradation in water

S. Mirehbar[a], S. Fernández-Velayos[a], E. Mazario[a], N. Menéndez[a], P. Herrasti[a], F.J. Recio[a,*], I. Sirés[b,**]

[a] *Departamento de Química Física Aplicada, Facultad de Ciencias, Universidad Autónoma de Madrid, C/Francisco Tomás y Valiente, 7, Cantoblanco, 28049 Madrid, Spain*

[b] *Laboratori d'Electroquímica dels Materials i del Medi Ambient, Departament de Química Física, Facultat de Química, Universitat de Barcelona, Martí i Franquès 1-11, 08028 Barcelona, Spain*

* Corresponding author, E-mail: javier.recioc@uam.es (Francisco Javier Recio)

** Corresponding author, E-mail: i.sires@ub.edu (Ignasi Sirés)

Abstract

Peroxydisulfate (PDS, $S_2O_8^{2-}$)-based advanced oxidation processes have been developed as an alternative to those based on $^{\bullet}OH$, as PDS activation yields a much more stable radical like $SO_4^{\bullet-}$ that can maintain the oxidation ability of water treatment systems for longer time. Here, the electrochemical PDS activation has been investigated using reticulated vitreous carbon (RVC) substrate modified with Fe_3O_4 nanoparticles (NPs) as cathode. The NPs were exhaustively characterized by different surface analysis techniques (TEM, SEM) and Mössbauer spectroscopy. Cyclic voltammetry and linear sweep voltammetry with a rotating disk electrode allowed concluding that the main electrocatalytic role in the cathodic PDS activation to $SO_4^{\bullet-}$ corresponded to the Fe(II) active sites continuously promoted upon cathodic polarization. These sites were less catalytic for O_2 reduction reaction, although it was still feasible with n = 2.7 electrons as determined from Koutecky-Levich analysis. Both cathodic reactions followed an inner-sphere reaction mechanism. The Fe_3O_4-modified RVC cathodes were employed to electrolyze Methylene Blue aqueous solutions at pH 3.5, employing different current values and PDS concentrations. Dissolved O_2 was purged to impede the competitive cathodic H_2O_2 production and Fenton's reaction. The occurrence of dye adsorption/electrosorption on the cathode reduced the mass transport limitations, enhancing the reaction between $SO_4^{\bullet-}$ and organic molecules. The best operation conditions to reach total and fast color removal at 18 min were 2 mM PDS and 10 mA, yielding > 80% TOC abatement at 45 min. Reproducible degradation profiles were found after 5 runs, thereby ensuring the stability of the Fe_3O_4-modified RVC, with no iron sludge production.

Keywords: Electrochemical advanced oxidation process; Methylene Blue; Persulfate; Reticulated vitreous carbon; Sulfate radical

1. Introduction

In the last few decades, the overgrowth of human population has entailed the massive entry of organic pollutants in all of the environmental compartments, being especially worrisome their accumulation in water because it is an essential ingredient for life. In the present study, Methylene Blue (MB) has been chosen as a model organic pollutant. MB is a fluorescent cationic dye discovered in 1876 [1], with multiple applications nowadays. For example, in medicine it serves for treating illnesses, microbiological staining or intraoperative imaging [1,2], whereas in the textile industry a great surplus of MB is discharged into wastewater effluents due to its poor adhesion to fabrics [3]. Such dye wastewater has become a major environmental issue in countries with intensive dyeing activities, since MB has a high molar absorptivity that causes aesthetic impact and limits the light penetration into water bodies [4]. Furthermore, the presence of MB in water is reported to cause negative health effects like high blood pressure, nausea, gastrointestinal irritation, skin irritation and abdominal pain [5].

More effective strategies for dye removal from water, not simply implying physical separation but their structural degradation, are thus needed. Outstanding results have been obtained for water and wastewater decontamination by means of advanced oxidation process (AOPs), which are particularly suitable for the degradation of organic pollutants. Classically, the high effectiveness of AOPs has been related to the generation of $^{\bullet}OH$ onsite [6,7], although the important contribution of $O_2^{\bullet-}$ and singlet oxygen under some experimental conditions has been increasingly discussed [8]. Lately, AOPs based on the action of sulfate radical anion ($SO_4^{\bullet-}$) have been developed as a viable alternative or complement to $^{\bullet}OH$-based AOPs [9,10]. Despite the lower redox potential of sulfate radical ($E^0(SO_4^{\bullet-}|SO_4^{2-}$ =

+2.437 ± 0.019 vs. SHE < E^0($^\bullet$OH|H_2O) = +2.730 ± 0.017 V vs. SHE) [11], its half-life is orders of magnitude longer (30-40 μs vs. 0.02 μs) [12,13], which makes $SO_4^{\bullet-}$ more readily diffused than $^\bullet$OH, also evidencing a higher selectivity towards organic matter oxidation. Note, however, that in aqueous matrices both radicals coexist, although $SO_4^{\bullet-}$ prevails as main oxidant over $^\bullet$OH at pH < 7 [14].

Within this context, electrochemistry has found a niche by giving rise to the so-called electrochemical AOPs [15,16]. The accurate modulation of the electrolysis conditions allows the in-situ electrosynthesis of oxidants like H_2O_2 [17-19] and peroxydisulfate (PDS, $S_2O_8^{2-}$) [20,21]. These species may act as precursors that can be further activated to yield $^\bullet$OH and $SO_4^{\bullet-}$, respectively. The excellent performance of both radicals related to color removal from dye solutions has been widely reported [22-24], as also verified for MB solutions [25].

In electrochemical systems, PDS can be activated through multiple routes: (i) Energy input from ultrasounds, microwaves, UV light or heat, as exemplified in reaction (1) for the thermal activation of persulfate (TAP) that can be accomplished using a water bath [26], a hot plate [27] or a solar thermal equipment [28]; (ii) reaction (2) in the presence of organic molecules (R); (iii) reaction (3) with low valence transition metal ions (M^{n+}) [29-31] such as Fe^{2+} [32,33]; and (iv) reactions (4) and (5) with electrogenerated H_2O_2 [34] or with its derived homogeneous radical, $^\bullet$OH, respectively [34].

$$S_2O_8^{2-} + \text{Heat} \rightarrow 2\ SO_4^{\bullet-} \quad (1)$$

$$S_2O_8^{2-} + R \rightarrow 2\ SO_4^{\bullet-} + R^\bullet \quad (2)$$

$$S_2O_8^{2-} + M^{n+} \rightarrow SO_4^{\bullet-} + M^{n+1} + SO_4^{2-} \quad (3)$$

$$S_2O_8^{2-} + H_2O_2 \rightarrow 2\ SO_4^{\bullet-} + 2\ ^\bullet OH \quad (4)$$

$$S_2O_8^{2-} + {}^\bullet OH \rightarrow SO_4^{\bullet-} + HSO_4^- + \tfrac{1}{2}\ O_2 \quad (5)$$

In addition to those five routes, the electrochemical activation of persulfate (EAP) is also feasible depending on the electrode materials. For example, reaction (5) could be alternatively mediated by M(•OH), an adsorbed radical formed from water oxidation at the surface of a large O_2-overpotential anode M like BDD [17,24] or PbO_2 [35,36]. The direct anodic oxidation of PDS at the anode surface has also been discussed in the literature, although this is still controversial because some authors suggest that PDS is actually activated to a nonradical transition state that oxidizes water to •OH [37,38]. On the other hand, the cathodic route has been much less explored so far [39]. Several scholars hypothesized the direct reduction of PDS at electrocatalytic surfaces via reaction (6) [31], as reported for Pt [40,41], stainless steel [42] and glassy carbon (GC) [43]. Nonetheless, these works do not demonstrate the occurrence of direct electron transfer. On a cathode made of carbon nanotubes, a nonradical PDS activation was observed [44]. In a much more thorough study that included voltammetric measurements and electrolysis in a divided cell, the cathodic PDS reduction to $SO_4^{\bullet -}$ was evidenced [45]. In that work, an irreversible reduction peak at Pt and graphite cathodes suggested the occurrence of direct cathodic activation.

$$S_2O_8^{2-} + e^- \rightarrow SO_4^{\bullet -} + SO_4^{2-} \quad (6)$$

Among the different strategies to enhance the electron transfer to/from an electrode in the EAP approach, the use of three-dimensional materials to expose a greater surface area should be seriously considered. Porous carbons like graphite felt and reticulated vitreous carbon are employed as substrates in many electrochemical applications [46,47], and different surface modification procedures allowed enhancing their performance very significantly, as shown by us for the treatment of organic pollutants [35,36,48]. A second finding to take into consideration is the proven effectiveness of the iron-based materials for

105 PS activation, although the mechanism is still under discussion due to controversy [49].
106 Magnetite (Fe_3O_4), which has an inverse spinel cubic structure, has been tested as
107 heterogeneous catalyst in the form of suspended nanoparticles (NPs) in solution for
108 peroxymonosulfate activation [50], whereas PDS has been activated by Fe_3O_4-α-MnO_2 NPs
109 [51] as well as by composites made of Fe_3O_4 particles embedded into Camellia seed husk-
110 based biochar that allowed the simultaneous adsorption and catalysis [52]. Some authors also
111 tested the electrochemical degradation of organic pollutants in the presence of suspended
112 Fe_3O_4 NPs, aiming to enhance the Fe(III) cathodic reduction [53], although this required a
113 previous adsorption on the catalyst surface.

114 In this work, PDS electroreduction has been investigated using RVC substrates modified
115 with Fe_3O_4 NPs, which have been exhaustively characterized by different surface analysis
116 techniques. The first goal was to discern whether the main electrocatalytic role in PDS
117 activation corresponded to the surface Fe(II) sites continuously promoted upon cathodic
118 polarization, which was assessed by means of cyclic voltammetry and linear polarization on
119 a rotating disk electrode (RDE). At the moment, there exists no strong evidence in the
120 literature on the Fe_3O_4-mediated PDS electroreduction using supported NPs. Afterwards, the
121 Fe_3O_4-modified RVC cathodes were employed to electrolyze MB aqueous solutions at
122 constant applied current (I_{app}) in the presence of different concentrations of PDS, trying to
123 find the best operation conditions for total color removal. The solution TOC was also
124 analyzed during these trials.

2. Experimental

2.1. Chemical compounds

MB is a heterocyclic aromatic dye with a thiazine structure (see molecular structure in Fig. S1). Its hydrated formed (molecular formula $C_{16}H_{18}ClN_3S{\bullet}H_2O$, > 95% purity, Sigma-Aldrich) was employed. Sodium persulfate ($Na_2S_2O_8$), and sodium sulfate (Na_2SO_4) of analytical grade were purchased from Panreac. Other solid and liquid chemicals were acquired from Sigma-Aldrich. High purity Milli-Q water with resistivity > 18.2 MΩ cm at 25 °C was used to prepare all the solutions.

2.2. Synthesis and characterization of magnetite nanoparticles

Fe_3O_4 NPs were synthesized using an electrochemical flow reactor operated in recirculation batch mode [54]. Eight iron electrodes were used as cathodes and anodes (area of 45 cm^2). The synthesis was carried out for 1 h at a constant I_{app} = 0.7 A in a 40 mM NaCl solution. The obtained NPs were separated magnetically as they were formed, being further rinsed with Milli-Q water several times until the supernatant was colorless. This simple and economic methodology allowed obtaining an estimated yield of 1 g NPs per hour.

The synthetized NPs were dried under vacuum overnight and their morphology was analyzed by transmission electron microscopy (TEM) using a JEOL JEM 1010 microscope operated at 100 kV. The average size of the NPs were determined upon measurement of at least 100 particles. The iron composition was determined by Mössbauer spectroscopy. Mössbauer spectra were recorded at room temperature in triangular mode using an emission spectrometer equipped with a ^{57}Co/Rh source. The spectral analyses were performed via a non-linear adjustment, using the NORMOS program [55], and energy calibrations were accomplished with an α-Fe foil (6 μm).

148 *2.3. Preparation and characterization of Fe_3O_4-modified RVC electrodes*

149 RVC foam (45 ppi, ULTRAMET) was modified with the synthetized Fe_3O_4 NPs
150 following a dip coating procedure. The RVC pieces were perfectly cut into dimensions of 70
151 mm × 20 mm × 10 mm (reproducible bare electrode mass of 1.8 ± 0.4 g, and volumetric
152 surface area of 30 cm^{-1}). The pieces were subsequently washed with acetone and water, and
153 then entirely submerged into a colloidal suspension of Fe_3O_4 NPs (10 g L^{-1}) for 30 min under
154 sonication, employing a Bandelin ultrasonic bath DT 100 H Sonorex Digitec (maximum
155 power of 320 W) with heating. The obtained electrodes were washed with Milli-Q water and
156 dried at 60 °C for 12 h. The mass of deposited NPs was practically constant (60 ± 5 mg).

157 The morphology of bare and modified RVC electrodes were characterized by scanning
158 electron microscopy (SEM) using a Hitachi S-3000N microscope. The equipment offered a
159 resolution of 3 nm at 25 kV and a tension range of 0.3 to 30 kV with an environmental
160 secondary electron detector (ESED) coupled to an Oxford Instruments energy dispersive X-
161 ray analyzer (model INCA x-sight).

162 *2.4. Electrochemical characterization and bulk electrolytic trials*

163 The electrochemical measurements were conducted on a GC RDE (geometrical area of
164 0.196 cm^2) from PINE Instruments as working electrode, since it is considered a valid model
165 surface to obtain data comparable with RVC. In most cases, the GC was further modified
166 with an ink made of Fe_3O_4 NPs and Vulcan XC-72 carbon black, which was prepared by
167 thoroughly mixing 2 mg of NPs and 2 mg of carbon and further hand-milling with an agate
168 mortar. The resulting powder was dispersed through sonication (same aforementioned bath)
169 in a beaker containing 1 mL of isopropanol and 4 mL of Milli-Q water. Then, 20 μL of Nafion
170 (5 wt.% in alcohol, Sigma-Aldrich) were added and the mixture was sonicated for 30 min to

ensure its homogeneity. The NPs concentration in the inks was set to ~0.5 mg mL^{-1}. The GC electrode surface was modified by dropping 20 μL of the ink and then dried under N_2 flow.

The electrochemical tests were carried out with an Autolab 302N potentiostat/galvanostat (Metrohm) controlled with Nova 2.0 software. A conventional three-electrode cell that contained a bare or modified GC RDE as working electrode, as well as an Ag|AgCl (saturated KCl) and a graphite rod as reference and counter electrode, respectively, was used. All the potentials in this work are referred to the reversible hydrogen electrode (RHE) under standard conditions, which agrees with the following expression: E(RHE) = E(Ag|AgCl (sat. KCl)) + 0.190 + 0.059pH. The electrochemical characterization was conducted by cyclic voltammetry in an N_2-saturated supporting electrolyte (0.1 M Na_2SO_4 solution prepared in Milli-Q water and adjusted to pH 3.5 with H_2SO_4). The oxygen reduction reaction (ORR) tests were performed by linear polarization in the same supporting electrolyte but saturated with O_2, at different rotation rates (ω), and the number of electrons was determined from the Koutecky-Levich equation [56]. The persulfate reduction was investigated in an O_2- or N_2-saturated electrolyte solution in the presence of 2 mM PDS, at ω = 1600 rpm. All voltammograms were recorded at a scan rate (v) of 5 mV s^{-1}.

The degradation experiments were performed in batch using an undivided glass reactor (120 mm in height × 60 mm in diameter). Mechanical stirring with PTFE blade impellers at 650 rpm was applied in all the experiments to ensure good mixing. A constant N_2 flow was always fed to the solutions in order to avoid the ORR contribution. Bare or Fe_3O_4-modified RVC (dimensions of 50 mm × 20 mm × 10 mm corresponded to the immersed part) were used as the cathode and graphite rod (70 mm in length × 6 mm in diameter) as the anode. To ensure the electric contact between the working electrode and the potentiostat, a graphite rod

was fixed to the RVC piece with silver conductive paint. The electrodes were connected to the abovementioned potentiostat/galvanostat, which supplied constant *I* of 5-15 mA in DC mode. The bulk electrolyses were performed with solutions of 200 mL containing 50 mg L^{-1} MB (i.e., 0.15 mM MB, total organic carbon (TOC) = 30 mg L^{-1}) and 50 mM Na_2SO_4 at pH 3.5. When needed, sodium persulfate was added to the MB solution just before supplying *I*, at a concentration of 1-6 mM.

The absorbance decay of the MB solutions was determined by UV/Vis spectroscopy on a Perkin-Elmer LAMBDA 35 UV/Vis spectrophotometer set at λ_{max} = 662–663 nm (see UV/Vis spectrum in Fig. S1). The solution decolorization has been expressed as follows [32]:

$$\%\ \text{Color removal} = \frac{A_0 - A_t}{A_0} \times 100 \quad (7)$$

where A_0 and A_i account for the solution absorbance at 0 min and at time *t*. Some reuse tests were comparatively performed by submerging the cathode in milli-Q water for 1 h after stopping the current supplied for the dye treatment. The solution TOC was analyzed at selected time intervals employing a TOC analyzer from Shimadzu (model VCSH).

3. Results and discussion

3.1. Characterization of Fe_3O_4 nanoparticles and RVC electrodes

The morphology of the Fe_3O_4 NPs synthesized in an electrochemical flow cell as explained in subsection 2.2 is shown in Fig. 1a, evidencing a quasi-spherical shape with a certain degree of aggregation. A mean diameter of 21 ± 7 nm has been determined by measuring this value from at least 100 particles observed in the different micrographs acquired. The standard deviation value informs about a moderate polydispersity of the NPs produced in recirculation mode. The Mössbauer spectrum of the synthesized NPs at 300 K

can be observed in Fig. 1b. A typical hyperfine pattern consisting of two overlapping six-line magnetic subspectra is depicted, yielding the following hyperfine parameters: IS = 0.556 (4) mm s^{-1} and the magnetic hyperfine field H = 44.64(4) T assignable to ^{57}Fe in the tetrahedral position; and IS = 0.329 (2) mm s^{-1} and H = 48.50(1) T related to the octahedral sites of the spinel lattice. The magnetic hyperfine values are slightly inferior to the ones corresponding to magnetite bulk material, but similar to reported values of Fe_3O_4 NPs with a diameter of 19 nm [57], thereby confirming the predominant magnetite structure in the electrochemically synthetized sample.

Before modifying the RVC substrate with the Fe_3O_4 NPs just characterized, the morphology of the bare RVC (45 ppi) was observed by SEM. Fig. 1c shows a pore size of about 500-600 µm, in good agreement with the porosity value provided by the manufacturer. SEM also served to corroborate the efficient deposition and homogeneous distribution of the particles. The surface analysis of the Fe_3O_4-modified RVC (Fig. 1d) allows confirming that 30 min of dip coating is a suitable duration to obtain a sufficiently uniform coating of the substrate. It is evident that the coating is rough the NPs are well distributed throughout the surface.

3.2. Electrochemical activation of PDS

A GC RDE, either bare or modified with the Fe_3O_4 NPs, was employed as the working electrode in a three-electrode cell to carry out these tests. The electrochemical characterization of the Fe_3O_4 NPs was first performed by cyclic voltammetry in an N_2-saturated 0.1 M Na_2SO_4 solution at pH 3.5. Fig. 2a shows the voltammogram obtained with the Fe_3O_4-modified GC RDE, which presents an electrochemically irreversible Faradaic process that can be related to the Fe(III)/Fe(II) redox process on the NPs surface. The anodic

239 and cathodic peak potentials appear at 0.79 and 0.31 V vs. RHE, respectively. Note that a
240 similar irreversible behavior has been reported for magnetite and ferrite NPs in acid media
241 [58]. The cathodic process can be represented as follows:

242 $\equiv Fe(III) + e^- \rightarrow \equiv Fe(II)$ (8)

243 where ≡ representes the solid state.

244 The electrocatalytic activity of the Fe_3O_4 NPs has been further studied in terms of
245 promotion and/or enhancement of both, PDS and O_2 reduction reactions. In particular, in
246 PDS-based AOPs the ORR can become a relevant simultaneous phenomenon during the
247 degradation of organic pollutants, since it can favor the occurrence of heterogeneous electro-
248 Fenton (EF) process as dissolved O_2 may yield H_2O_2 as Fenton's reactant in the presence of
249 adsorbed Fe_3O_4 NPs [15,17,19]. As can be observed in Fig. 2a, a comparison between the
250 polarization curves with bare and Fe_3O_4-modified GC allows concluding that the NPs are
251 active for both reduction reactions. This is readily deduced from the clear decrease in the
252 onset potential for both reactions using the modified working electrode. An additional and
253 very remarkable finding, as evidenced by comparing both reduction signals using the same
254 modified electrode, is the greater electroactivity of Fe_3O_4 towards PDS reduction. The
255 corresponding onset potential was 0.150 V more positive as compared to the ORR.
256 Furthermore, the onset potential for each reaction appears in the region related to the cathodic
257 process assigned to the Fe(III) to Fe(II) conversion previously observed in the cyclic
258 voltammogram (reaction (8)). Therefore, this is an evidence of cathodic O_2 reduction and
259 PDS activation (reaction (9), 1st step) mediated by electrogenerated Fe(II) sites. The latter
260 process mimics the more commonly reported PDS activation in solution (reaction (3)) [32];
261 however, in solution reaction there is a gradual accumulation of Fe^{3+}, whereas with the

immobilized NPs the cathodic polarization becomes essential because it ensures that the iron centers remain continuously available as Fe(II), as illustrated in the equilibrium shown in reaction (9) (2^{nd} step).

$$S_2O_8^{2-} + \equiv Fe(II) \rightarrow \equiv Fe(III) + SO_4^{\bullet-} + SO_4^{2-} \leftrightarrow \equiv Fe(II) + SO_4^{\bullet-} + SO_4^{2-} \quad (9)$$

The occurrence of reaction (9) at Fe_3O_4 surface sites is potentially advantageous, since it avoids the need of dissolved metal cations like Fe^{2+} that tend to precipitate in aqueous solution if the pH is not sufficiently acid. Hence, the absence of iron sludge production directly reduces the cost and time associated to its management.

The direct connection found between the Fe(III)/Fe(II) redox potential and the onset potential for both reactions mentioned above implies an inner-sphere reaction mechanism, as previously proposed for the ORR catalyzed by ferrite NPs, iron-doped carbon materials and single atom molecular catalysts [59-61]. From this, it can be assured that O_2 and PDS must be adsorbed on the Fe(II) sites to start the electroreduction. The PDS reduction reaction presented diffusional control at low overpotentials (0.2 V vs. RHE, Fig. 2a); this phenomenon also occurred during the ORR, although at much greater overpotentials (-0.4 V vs. RHE, Fig. S2a) and attaining current values one order of magnitude higher as compared to PDS (not shown). The total number of electrons for the ORR has been determined via Koutecky-Levich analysis of data obtained from linear sweep voltammetries recorded at different rotation rates (Fig. S2a,b). The results highlight a mixed mechanism via 2.7 electrons, informing about the production of H_2O_2 as main product that could be further employed to stimulate Fenton's reaction during the treatment of aerated contaminated solutions.

Based on the latter finding, the presence of dissolved O_2 in aerated water effluents to be treated by PDS-based AOPs can lead to an overestimation of the oxidizing role of $SO_4^{\bullet-}$,

since H_2O_2 not only induces Fenton's reaction either with dissolved Fe^{2+} or anchored Fe(II) [15,62], but it also acts as PDS activator via reaction (4). In such scenario, the degradation of the organic molecules is expected to be caused by the combined action of both, $SO_4^{\bullet-}$ and $^{\bullet}OH$ [34,63]. Aiming to evaluate the influence of O_2, solutions containing 50 mg L^{-1} (0.15 mM) MB and 50 mM Na_2SO_4 at pH 3.5 were electrolyzed at I_{app} = 10 mA using an undivided reactor with an Fe_3O_4-modified RVC cathode and a graphite anode. The PDS-based process (i.e., $SO_4^{\bullet-}$ as main oxidant) was tested upon addition of 1 mM PDS to the N_2-saturated solution, whereas the heterogeneous EF process (i.e., $^{\bullet}OH$ as main oxidant) was performed under O_2 saturation without PDS. As highlighted in Fig. 2b, a high percentage of color removal was attained after 180 min by both treatments, being superior in the $^{\bullet}OH$-mediated process (90% vs. 80%) thanks to the greater redox potential of this radical as compared to $SO_4^{\bullet-}$. Nonetheless, the PDS-based treatment was comparatively more effective within the first minutes, as the maximum decolorization of 80% with PDS was already achieved at 2 min, a value significantly higher than 60% reached by EF. The slower initial MB degradation in the latter process can be accounted for by the absence of the $^{\bullet}OH$ precursor in the initial solution, since H_2O_2 must be electrogenerated on site, in contrast to the PDS process in which a fast activation to $SO_4^{\bullet-}$ is feasible from the beginning. Once a sufficiently high H_2O_2 concentration was accumulated (~90 min), the EF process became superior.

Additionally, note that in heterogeneous EF process, the Fe(II) active sites present on the deposited NPs surface are needed to catalyze two reactions to finally produce the $^{\bullet}OH$: the 2-electron ORR and the heterogeneous Fenton's reaction. Conversely, in the PDS-based AOP all the catalytic sites are available for $SO_4^{\bullet-}$ generation without requiring any intermediate whose formation could decelerate the degradation. From the trends of Fig. 2b,

it can then be concluded that even the decolorization of aerated solutions can be readily promoted by PDS alone, being the contribution of •OH less relevant, although these radical can become useful as the electrolysis is prolonged in order to reach a large percentage of TOC decay.

3.3. Focus on PDS-based advanced oxidation treatment of dye solutions

Iron-based NPs and hybrid materials haven been successfully employed in water decontamination promoted by the adsorption and magnetic separation of the organic pollutants [64-68]. To discern whether the adsorption and electrosorption of MB on the modified RVC cathode plays a significant role in the degradation process, N_2-saturated solutions containing 50 mg L^{-1} MB and 50 mM Na_2SO_4 at pH 3.5 without PDS were treated using the same reactor and electrodes described in the previous subsection. The effect of I_{app} on the percentage of color removal over time is depicted in Fig. 3a. The MB removal via purely physical adsorption (i.e., no applied current) upon contact of the stirred solution with the large surface area RVC cathode was negligible, reaching an average value as low as 3%. This behavior is attributed to the electrostatic repulsion between the MB and the surface of the Fe_3O_4 NPs; the isoelectric point of the particles (pI ~6.5) induced the appearance of a positive surface charge at pH 3.5, whereas at such solution pH the MB (pK_a = 3.8) was mainly protonated [64,69]. Note that Hung et al. [70] also reported that MB is believed to become adsorbed onto the surface of Fe_3O_4 NPs, which they employed as catalyst in non-electrochemical experiments.

The situation changed upon galvanostatic electrolysis, which induced an electroadsoption phenomenon that contributed to reach a certain degree of decolorization at all I_{app} tested. At 6 min, the color removal was 2%, 8%, 28% and 14% operating at 0, 5, 10

and 15 mA, respectively. The detrimental effect of current increase from 10 to 15 mA can be explained by a more ordered adsorption of the MB molecules onto the NPs and uncoated RVC, both on the surface and through the pores, at 10 mA; a higher cathodic current causes a faster migration of MB in its cationic form, facilitating a less ordered surface coverage that potentially blocks some of the pores during the first minutes. At 30 min, even at 10 mA the cathode coverage tended to reach a limit and hence, the percentage of color removal became similar (plateau around 37%-40%) at the two highest I_{app} values, being twice greater than that at 5 mA (18%).

To corroborate that the color loss evidenced in Fig. 3a was due to adsorption/electrosorption on the Fe_3O_4-modified RVC piece and not to transformation phenomena, a desorption test was performed at the end of the experiments at each I_{app} by immersing the cathode into Milli-Q water for 60 min under vigorous stirring. The TOC content of final solutions obtained from the treatment of MB solutions and from desorption trials was determined, as shown in Fig. 3b. It is evident that the concentration of organic carbon in the system remained constant regardless of the I_{app} value, which means that no mineralization occurred. However, the distribution of this TOC differed in each treatment, with maximum decay of dissolved TOC found at 10-15 mA, in agreement with maximum color removal under these conditions (Fig. 3a). From a practical point of view, the existence of adsorption phenomena is expected to be beneficial because the MB oxidation and mineralization will be accelerated thanks to the minimization of mass transport limitations.

A critical parameter in PDS-based AOPs is the PDS concentration, as this is the direct source of $SO_4^{\bullet-}$. N_2-saturated MB solutions as those mentioned for tests in Fig. 3 but containing 1-6 mM PDS were electrolyzed at I_{app} = 10 mA, using the same reactor and

electrodes. Fig. 4a illustrates an abrupt color decay at the beginning of all the experiments, whereupon the decolorization percentages stabilized until the end of the electrolysis. A minimum of 2 mM PDS was needed to gradually achieve 100% color removal, since the use of 1 mM PDS only allowed 80% (Fig. 2b). When a much greater reagent concentration of 6 mM was employed, a quicker total decolorization occurred at 2 min instead of 18 min, which suggests that the Fe_3O_4 NPs surface always contains a sufficiently high accessibility to Fe(II) sites to accelerate the production of $SO_4^{\bullet-}$ if enough PDS is fed to the cathode. However, it was also observed that such high PDS content became detrimental in terms of cathode durability, since the solution turbidity underwent an evident increase during the test with 6 mM PDS. After the test, clear damage of the modified RVC electrode was detected, entailing a decrease in its dimensions and a greater embrittlement that put its mechanical stability at risk. The degradation of the material could be associated with the high amount of $SO_4^{\bullet-}$ generated at the cathode surface, which induced the oxidation of the carbon.

Considering a balanced performance integrating both, solution decontamination and electrode stability, the effect of I_{app} was investigated under the conditions of Fig. 4a at 2 mM PDS. In Fig. 4b, it can be seen that the lowest I_{app} = 5 mA was able to yield complete color removal after 40 min in a gradual manner. The much slower degradation as compared to the test made at 10 mA (18 min) is mainly justified by the more limited regeneration of the Fe(II) active sites, which eventually decelerates the production of $SO_4^{\bullet-}$. Worth commenting, a preliminary test made with no current supply revealed a substantial tendency of MB to precipitate over time due to the action of PDS, which consequently led to the loss of PDS in the medium [71]. An increase of I_{app} to 15 mA did not yield further amelioration, only reaching a maximum color loss of 90-95%, maybe because an excessive production of $SO_4^{\bullet-}$

enhanced their self-decomposition through radical-radical reactions (see below). On the other hand, despite the similarities in the decolorization profiles, much clearer differences appeared during TOC analysis (TOC_0 ~30 mg L^{-1}). Fig. 4c presents the dissolved (direct measurement) and adsorbed (obtained upon desorption, see Fig. 3) TOC values after 45 min of each treatment shown in Fig. 4b, along with the corresponding TOC abatement percentage (i.e., TOC escaping the system upon mineralization). The electrolysis carried out at 5 mA allowed decreasing the TOC in solution to ~7.5 mg L^{-1}, with the organic matter adsorbed on the cathode accounting for ~5 mg L^{-1} TOC, which means that 58% of TOC_0 was effectively removed (i.e., mineralized to CO_2). The TOC abatement was greater (~83%) at the two highest I_{app} values, whose effect was similar and yielded final TOC values of ~3 and ~2 mg L^{-1} in solution and on RVC, respectively. It is interesting to highlight that, although at 15 mA the color removal was lower than that at 5 mA, its ability to promote the gradual degradation of the reaction byproducts was larger. It can then be inferred that at 15 mA, the excess of $SO_4^{\bullet-}$ mainly participated in the oxidation of byproducts.

Finally, in order to evaluate the reusability of a freshly prepared Fe_3O_4-modified RVC cathode, five consecutive degradation runs were performed under the conditions described in Fig. 4, at 2 mM PDS and I_{app} = 10 mA. Fig. 5a illustrates the percentage of color removal over time during the tests, evidencing a complete decolorization at 18 min in all cases, although in the 5th run the profile was slightly different and suggested a slower degradation that can be related to performance loss. The excellent behavior of the system after the 5 runs was further corroborated from TOC analysis. Quite reproducible dissolved and adsorbed TOC values were determined after each reuse under study (Fig. 5b), always accounting for more than 80% of mineralization.

4. Conclusions

This work demonstrates that the substantial enrichment of magnetite surface with Fe(II) sites during its cathodic polarization leads to the enhanced electrocatalysis of PDS and O_2 reduction as compared to bare carbon cathode. The Fe_3O_4 activity towards PDS activation was comparatively greater than that towards O_2. The heterogeneous conversion of PDS into $SO_4^{\bullet-}$ mimics the more conventional PDS activation by dissolved Fe^{2+}. This is clearly advantageous for practical application, since the sludge production typically associated to the precipitation of dissolved metal cations like Fe^{2+} and Fe^{3+} can be impeded. The viability of PDS-based treatments to degrade an organic molecule like MB dye in N_2-saturated medium has been proven, achieving a complete decolorization of solutions in short time upon optimization of the electrolysis conditions. TOC abatements greater than 80% were also attained after relatively short treatments. PDS concentration must not be too high or too low, since the electrode stability is compromised or the amount of $SO_4^{\bullet-}$ is insufficient, respectively. Further work should address the simultaneous heterogeneous EF process using dissolved O_2.

Acknowledgments

The authors kindly acknowledge financial support from projects PGC2018-095642-B-I00 (MINECO, Spain) and PID2019-109291RB-I00 (AEI, Spain). E. M. is grateful to the Madrid Government (Comunidad de Madrid, Spain) under the Multiannual Agreement with Universidad Autónoma de Madrid to encourage young research doctors within the context of the V PRICIT (Regional Program of Research and Technological Innovation, reference SI1-PJI-2019-00366).

References

[1] T. Cwalinski, W. Polom, L. Marano, G. Roviello, A. D'Angelo, N. Cwalina, M. Matuszewski, F. Roviello, J. Jaskiewicz, K. Polom, Methylene Blue—Current knowledge, fluorescent properties, and its future use, J. Clin. Med. 9(11) (2020) 3538. Doi: 10.3390/jcm9113538

[2] C. Ponraj, V.G., J. Daniel, A review on the visible light active $BiFeO_3$ nanostructures as suitable photocatalyst in the degradation of different textile dyes, Environ. Nanotechnol. Monit. Manage. 7 (2017) 110–120. Doi: 10.1016/j.enmm.2017.02.001

[3] A.M. Kosswattaarachchi, T.R. Cook, Repurposing the industrial dye Methylene Blue as an active component for redox flow batteries, ChemElectroChem 5 (2018) 3437–3442. Doi: 10.1002/celc.201801097

[4] F.A. Ozdemir, B.D.R. Apak, Adsorptive removal of methylene blue from simulated dyeing wastewater with melamine-formaldehyde-urea resin, J. Appl. Polym. Sci. 112 (2009) 3442–3448. Doi: 10.1002/app.29835

[5] H. Lyu, B. Gao, F. He, A.R. Zimmerman, C. Ding, J. Tang, J.C. Crittenden, Experimental and modeling investigations of ball-milled biochar for the removal of aqueous methylene blue, Chem. Eng. J. 335 (2018) 110–119. Doi: 10.1016/j.cej.2017.10.130

[6] M.A. Oturan, J.-J. Aaron, Advanced oxidation processes in water/wastewater treatment: Principles and applications. A review, Crit. Rev. Environ. Sci. Technol. 44 (2014) 2577–2641. Doi: 10.1080/10643389.2013.829765

443 [7] D.B. Miklos, C. Remy, M. Jekel, K.G. Linden, J.E. Drewes, U. Hübner, Evaluation of
444 advanced oxidation processes for water and wastewater treatment — A critical review,
445 Water Res. 139 (2018) 118–131. Doi: 10.1016/j.watres.2018.03.042
446 [8] J. Al-Nu'airat, I. Oluwoye, N. Zeinali, M. Altarawneh, B.Z. Dlugogorski, Review of
447 chemical reactivity of singlet oxygen with organic fuels and contaminants, Chem. Rec.
448 21 (2021) 315–342. Doi: 10.1002/tcr.202000143
449 [9] X. Duan, S. Yang, S. Wacławek, G. Fang, R. Xiao, D.D. Dionysiou, Limitations and
450 prospects of sulfate-radical based advanced oxidation processes, J. Environ. Chem.
451 Eng. 8 (2020) 103849. Doi: 10.1016/j.jece.2020.103849
452 [10] Z.-Y. Guo, C.-X. Li, M. Gao, X. Han, Y.-J. Zhang, W.-J. Zhang, W.-W. Li, Mn-O
453 covalency governs the intrinsic activity of Co-Mn spinel oxides for boosted
454 peroxymonosulfate activation, Angew. Chem. Int. Ed. 60 (2021) 274–280. Doi:
455 10.1002/anie.202010828
456 [11] D.A. Armstrong, R.E. Huie, S. Lymar, W.H. Koppenol, G. Merényi, P. Neta, D.M.
457 Stanbury, S. Steenken, P. Wardman, Standard electrode potentials involving radicals
458 in aqueous solution: inorganic radicals (IUPAC Technical Report), Pure Appl. Chem.
459 87 (2015) 1139–1150. Doi: 10.1515/pac-2014-0502
460 [12] A.K. Pikaev, V.I. Zolotarevskii, Pulse radiolysis of aqueous solutions of sulfuric acid,
461 Bull. Acad. Sci. USSR 16(1) (1967) 181–182. Doi: 10.1007/BF00907128
462 [13] X. Xia, F. Zhu, J. Li, H. Yang, L. Wei, Q. Li, J. Jiang, G. Zhang, Q. Zhao, A review
463 study on sulfate-radical-based advanced oxidation processes for domestic/industrial
464 wastewater treatment: Degradation, efficiency, and mechanism, Front. Chem. 8 (2020)
465 592056. Doi: 10.3389/fchem.2020.592056
466 [14] A. Romero, A. Santos, F. Vicente, C. González, Diuron abatement using activated

persulphate: effect of pH, Fe(II) and oxidant dosage, Chem. Eng. J. 162 (2010) 257–265. Doi: 10.1016/j.cej.2010.05.044

[15] E. Brillas, I. Sirés, M.A. Oturan, Electro-Fenton process and related electrochemical technologies based on Fenton's reaction chemistry, Chem. Rev. 109 (2009) 6570–6631. Doi: 10.1021/cr900136g

[16] C.A. Martínez-Huitle, M.A. Rodrigo, I. Sirés, O. Scialdone, Single and coupled electrochemical processes and reactors for the abatement of organic water pollutants: A critical review, Chem. Rev. 115 (2015) 13362–13407. Doi: 10.1021/acs.chemrev.5b00361

[17] A. Galia, S. Lanzalaco, M.A. Sabatino, C. Dispenza, O. Scialdone, I. Sirés, Crosslinking of poly(vinylpyrrolidone) activated by electrogenerated hydroxyl radicals: A first step towards a simple and cheap synthetic route of nanogel vectors, Electrochem. Commun. 62 (2016) 64–68. Doi: 10.1016/j.elecom.2015.12.005

[18] R. Salazar, J. Gallardo-Arriaza, J. Vidal, C. Rivera-Vera, C. Toledo-Neira, M.A. Sandoval, L. Cornejo-Ponce, A. Thiam, Treatment of industrial textile wastewater by the solar photoelectro-Fenton process: Influence of solar radiation and applied current, Solar Energy 190 (2019) 82–91. Doi: 10.1016/j.solener.2019.07.072

[19] G. Daniel, Y. Zhang, S. Lanzalaco, F. Brombin, T. Kosmala, G. Granozzi, A. Wang, E. Brillas, I. Sirés, C. Durante, Chitosan-derived nitrogen-doped carbon electrocatalyst for a sustainable upgrade of oxygen reduction to hydrogen peroxide in UV-assisted electro-Fenton water treatment, ACS Sustain. Chem. Eng. 8 (2020) 14425–14440. Doi: 10.1021/acssuschemeng.0c04294

[20] D. Medeiros de Araújo, C. Sáez, P. Cañizares, M.A. Rodrigo, C.A. Martínez-Huitle, Improving the catalytic effect of peroxodisulfate and peroxodiphosphate

electrochemically generated at diamond electrode by activation with light irradiation, Chemosphere 207 (2018) 774–780. Doi: 10.1016/j.chemosphere.2018.05.121

[21] K. Groenen-Serrano, A critical review on the electrochemical production and use of peroxo-compounds, Curr. Opin. Electrochem. 27 (2021) 100679. Doi: 10.1016/j.coelec.2020.100679

[22] O. Scialdone, A. Galia, C. Gattuso, S. Sabatino, B. Schiavo, Effect of air pressure on the electro-generation of H_2O_2 and the abatement of organic pollutants in water by electro-Fenton process, Electrochim. Acta 182 (2015) 775–780. Doi: 10.1016/j.electacta.2015.09.109

[23] A. Thiam. I. Sirés, E. Brillas, Treatment of a mixture of food color additives (E122, E124 and E129) in different water matrices by UVA and solar photoelectro-Fenton, Water Res. 81 (2015) 178–187. Doi: 10.1016/j.watres.2015.05.057

[24] S. Cotillas, J. Llanos, P. Cañizares, D. Clematis, G. Cerisola, ;.A. Rodrigo, M. Panizza, Removal of Procion Red MX-5B dye from wastewater by conductive-diamond electrochemical oxidation, Electrochim. Acta 263 (2018) 1–7. Doi: 10.1016/j.electacta.2018.01.052

[25] M. Panizza, A. Barbucci, R. Ricotti, G. Cerisola, Electrochemical degradation of methylene blue, Sep. Purif. Technol. 54 (2007) 382–387. Doi: 10.1016/j.seppur.2006.10.010

[26] C. Liang, H.-W. Su, Identification of sulfate and hydroxyl radicals in thermally activated persulfate, Ind. Eng. Chem. Res. 48 (2009) 5558–5562. Doi: 10.1021/ie9002848

513 [27] C.M. Dominguez, A. Romero, D. Lorenzo, A. Santos, Thermally activated persulfate
514 for the chemical oxidation of chlorinated organic compounds in groundwater, J.
515 Environ. Manage. 261 (2020) 110240. Doi: 10.1016/j.jenvman.2020.110240
516 [28] C. Telegang Chekem, S. Chiron, J.M. Mancaux, G. Plantard, V. Goetz, Thermal
517 activation of persulfates for wastewater depollution on pilot scale solar equipment,
518 Solar Energy 205 (2020) 372–379. Doi: 10.1016/j.solener.2020.04.075
519 [29] D.A. House, Kinetics and mechanism of oxidations by peroxydisulfate, Chem. Rev.
520 62 (1962) 185–203. Doi: 10.1021/cr60217a001
521 [30] G.V. Buxton, T.N. Malone, G. Arthur Salmon, Reaction of SO_4^- with Fe^{2+}, Mn^{2+} and
522 Cu^{2+} in aqueous solution, J. Chem. Soc. Faraday Trans. 93 (1997) 2893–2897. Doi:
523 10.1039/A701472D
524 [31] S.A. Shafiee, J. Aarons, H.H. Hamzah, Review—Electroreduction of peroxodisulfate:
525 A review of a complicated reaction, J. Electrochem. Soc. 165 (2018) H785–H798.
526 Doi: 10.1149/2.1161811jes
527 [32] A.J. dos Santos, I. Sirés, E. Brillas, Removal of bisphenol A from acidic sulfate
528 medium and urban wastewater using persulfate activated with electroregenerated Fe^{2+},
529 Chemosphere 263 (2021) 128271. Doi: 10.1016/j.chemosphere.2020.128271
530 [33] Z. Sun, S. Li, H. Ding, Y. Zhu, X. Wang, H. Liu, Q. Zhang, C. Zhao,
531 Electrochemical/Fe^{3+}/peroxymonosulfate system for the degradation of Acid Orange
532 7 adsorbed on activated carbon fiber cathode, Chemosphere. 241 (2020) 125125. Doi:
533 10.1016/j.chemosphere.2019.125125
534 [34] A.J. dos Santos, E. Brillas, P.L. Cabot, I. Sirés, Simultaneous persulfate activation by
535 electrogenerated H_2O_2 and anodic oxidation at a boron-doped diamond anode for the

536 treatment of dye solutions, Sci. Total Environ. 747 (2020) 141541. Doi:
537 10.1016/j.scitotenv.2020.141541
538 [35] F.J. Recio, P. Herrasti, I. Sirés, A.N. Kulak, D. V Bavykin, C. Ponce-de-León, F.C.
539 Walsh, The preparation of PbO_2 coatings on reticulated vitreous carbon for the electro-
540 oxidation of organic pollutants, Electrochim. Acta. 56 (2011) 5158–5165. Doi:
541 10.1016/j.electacta.2011.03.054
542 [36] G. Ramírez, F.J. Recio, P. Herrasti, C. Ponce-de-León, I. Sirés, Effect of RVC porosity
543 on the performance of PbO_2 composite coatings with titanate nanotubes for the
544 electrochemical oxidation of azo dyes, Electrochim. Acta. 204 (2016) 9–17. Doi:
545 10.1016/j.electacta.2016.04.054
546 [37] J. Cai, T. Niu, P. Shi, G. Zhao, Boron-doped diamond for hydroxyl radical and sulfate
547 radical anion electrogeneration, transformation, and voltage-free sustainable oxidation,
548 Small 15 (2019) 1900153. Doi: 10.1002/smll.201900153
549 [38] H. Song, L. Yan, Y. Wang, J. Jiang, J. Ma, C. Li, G. Wang, J. Gu, P. Liu,
550 Electrochemically activated PMS and PDS: Radical oxidation versus nonradical
551 oxidation, Chem. Eng. J. 391 (2020) 123560. Doi: 10.1016/j.cej.2019.123560
552 [39] D. Zhi, Y. Lin, L. Jiang, Y. Zhou, A. Huang, J. Yang, L. Luo, Remediation of
553 persistent organic pollutants in aqueous systems by electrochemical activation of
554 persulfates: A review, J. Environ. Manage. 260 (2020) 110125. Doi:
555 10.1016/j.jenvman.2020.110125
556 [40] W.-S. Chen, Y.-C. Jhou, C.-P. Huang, Mineralization of dinitrotoluenes in industrial
557 wastewater by electro-activated persulfate oxidation, Chem. Eng. J. 252 (2014) 166–
558 172. Doi: 10.1016/j.cej.2014.05.033
559 [41] W.-S. Chen, C.-P. Huang, Mineralization of aniline in aqueous solution by

560 electrochemical activation of persulfate, Chemosphere 125 (2015) 175–181. Doi:
561 10.1016/j.chemosphere.2014.12.053
562 [42] J. Wu, H. Zhang, J. Qiu, Degradation of Acid Orange 7 in aqueous solution by a novel
563 electro/Fe^{2+}/peroxydisulfate process, J. Hazard. Mater. 215-216 (2012) 138–145. Doi:
564 10.1016/j.jhazmat.2012.02.047
565 [43] H. Zeng, S. Liu, B. Chai, D. Cao, Y. Wang, X. Zhao, Enhanced photoelectrocatalytic
566 decomplexation of Cu-EDTA and Cu recovery by persulfate activated by UV and
567 cathodic reduction, Environ. Sci. Technol. 50 (2016) 6459–6466. Doi:
568 10.1021/acs.est.6b00632
569 [44] C. Nie, Z. Ao, X. Duan, C. Wang, S. Wang, T. An, Degradation of aniline by
570 electrochemical activation of peroxydisulfate at MWCNT cathode: The proofed
571 concept of nonradical oxidation process, Chemosphere 206 (2018) 432–438. Doi:
572 10.1016/j.chemosphere.2018.04.173
573 [45] L.W. Matzek, M.J. Tipton, A.T. Farmer, A.D. Steen, K.E. Carter, Understanding
574 electrochemically activated persulfate and its application to ciprofloxacin abatement,
575 Environ. Sci. Technol. 52(10) (2018) 5875–5883. Doi: 10.1021/acs.est.8b00015
576 [46] F.C. Walsh, L.F. Arenas, C. Ponce de León, G.W. Reade, I. Whyte, B.G. Mellor, The
577 continued development of reticulated vitreous carbon as a versatile electrode material:
578 Structure, properties and applications, Electrochim. Acta 215 (2016) 566–591. Doi:
579 10.1016/j.electacta.2016.08.103
580 [47] L.F. Castañeda, F.C. Walsh, J.L. Nava, C. Ponce de León, Graphite felt as a versatile
581 electrode material: Properties, reaction environment, performance and applications,
582 Electrochim. Acta 258 (2017) 1115–1139. Doi: 10.1016/j.electacta.2017.11.165
583 [48] I. Sirés, C.T.J. Low, C. Ponce-de-León, F.C. Walsh, The deposition of nanostructured

584 β-PbO_2 coatings from aqueous methanesulfonic acid for the electrochemical oxidation
585 of organic pollutants, Electrochem. Commun. 12 (2010) 70–74. Doi:
586 10.1016/j.elecom.2009.10.038
587 [49] K. Hou, Z. Pi, F. Yao, B. Wu, L. He, X. Li, D. Wang, H. Dong, Q. Yang, A critical
588 review on the mechanisms of persulfate activation by iron-based materials: Clarifying
589 some ambiguity and controversies, Chem. Eng. J. 407 (2021) 127078. Doi:
590 10.1016/j.cej.2020.127078
591 [50] J. Liu, J. Zhou, Z. Ding, Z. Zhao, X. Xu, Z, Fang, Ultrasound irritation enhanced
592 heterogeneous activation of peroxymonosulfate with Fe_3O_4 for degradation of azo dye,
593 Ultrason. Sonochem. 34 (2017) 953–959. Doi: 10.1016/j.ultsonch.2016.08.005
594 [51] Z. Dong, Q. Zhang, B.-Y. Chen, J. Hong, Oxidation of bisphenol A by persulfate via
595 Fe_3O_4-α-MnO_2 nanoflower-like catalyst: Mechanism and efficiency, Chem. Eng. J.
596 357 (2019) 337–347. Doi: 10.1016/j.cej.2018.09.179
597 [52] Z. Pi, X. Li, D. Wang, Q. Xu, Z. Tao, X. Huang, F. Yao, Y. Wu, L. He, Q. Yang,
598 Persulfate activation by oxidation biochar supported magnetite particles for
599 tetracycline removal: Performance and degradation pathway, J. Cleaner Prod. 235
600 (2019) 1103–1115. Doi: 10.1016/j.jclepro.2019.07.037
601 [53] H. Lin, H. Zhang, L. Hou, Degradation of C. I. Acid Orange 7 in aqueous solution by
602 a novel electro/Fe_3O_4/PDS process, J. Hazard. Mater. 276 (2014) 182–191. Doi:
603 10.1016/j.jhazmat.2014.05.021
604 [54] I. Lozano, C. López, N. Menendez, N. Casillas, P. Herrasti, Design, construction and
605 evaluation of a 3D printed electrochemical flow cell for the synthesis of magnetite
606 nanoparticles, J. Electrochem. Soc. 165 (2018) H688–H697. Doi:

10.1149/2.1401810jes

[55] R.A. Brand, Improving the validity of hyperfine field distributions from magnetic alloys, Nucl. Instruments Methods Phys. Res. Sect. B: Beam Interact. with Mater. Atoms 28 (1987) 398–416. Doi: 10.1016/0168-583X(87)90182-0

[56] F. Alcaide, G. Álvarez, D.R.V. Guelfi, E. Brillas, I. Sirés, A stable CoSP/MWCNTs air-diffusion cathode for the photoelectro-Fenton degradation of organic pollutants at pre-pilot scale, Chem. Eng. J. 379 (2020) 122417. Doi: 10.1016/j.cej.2019.122417

[57] K. Woo, J. Hong, S. Choi, H.-W. Lee, J.-P. Ahn, C.S. Kim, S.W. Lee, Easy synthesis and magnetic properties of iron oxide nanoparticles, Chem. Mater. 16 (2004) 2814–2818. Doi: 10.1021/cm049552x

[58] J.J.P. Roberts, J.A. Westgard, L.M. Cooper, R.W. Murray, Solution voltammetry of 4 nm magnetite ion oxide nanoparticles, J. Am. Chem. Soc. 136 (2014) 10783–10789. Doi: 10.1021/ja505562p

[59] H. Zhu, S. Zhang, Y.-X. Huang, L. Wu, S. Sun, Monodisperse $M_xFe_{3-x}O_4$ (M = Fe, Cu, Co, Mn) nanoparticles and their electrocatalysis for oxygen reduction reaction, Nano Lett. 13 (2013) 2947–2951. Doi: 10.1021/nl401325u

[60] J.H. Zagal, F. Javier Recio, C.A. Gutierrez, C. Zuñiga, M.A. Páez, C.A. Caro, Towards a unified way of comparing the electrocatalytic activity MN_4 macrocyclic metal catalysts for O_2 reduction on the basis of the reversible potential of the reaction, Electrochem. Commun. 41 (2014) 24–26. Doi: 10.1016/j.elecom.2014.01.009

[61] R. Venegas, K. Muñoz-Becerra, C. Candia-Onfray, J.F. Marco, J.H. Zagal, F.J. Recio, Experimental reactivity descriptors of M-N-C catalysts for the oxygen reduction reaction, Electrochim. Acta 332 (2020) 135340. Doi: 10.1016/j.electacta.2019.135340

[62] Y. Zhang, G. Daniel, S. Lanzalaco, A.A. Isse, A. Facchin, A. Wang, E. Brillas, C.

631 Durante, I. Sirés, H_2O_2 production at gas-diffusion cathodes made from agarose-
632 derived carbons with different textural properties for acebutolol degradation in
633 chloride media, J. Hazard. Mater. 423 (2022) 127005. Doi:
634 10.1016/j.jhazmat.2021.127005
635 [63] H. Luo, Y. Cheng, Y. Zeng, K. Luo, D. He, X. Pan, Rapid removal of organic
636 micropollutants by heterogeneous peroxymonosulfate catalysis over a wide pH range:
637 Performance, mechanism and economic analysis, Sep. Purif. Technol. 248 (2020)
638 117023. Doi: 10.1016/j.seppur.2020.117023
639 [64] H. Paudyal, B. Pangeni, K. Inoue, H. Kawakita, K. Ohto, H. Harada, S. Alam,
640 Adsorptive removal of fluoride from aqueous solution using orange waste loaded with
641 multi-valent metal ions, J. Hazard. Mater. 192 (2011) 676–682. Doi:
642 10.1016/j.jhazmat.2011.05.070
643 [65] O. Duman, S. Tunç, T.G. Polat, B.K. Bozoğlan, Synthesis of magnetic oxidized
644 multiwalled carbon nanotube-κ-carrageenan-Fe_3O_4 nanocomposite adsorbent and its
645 application in cationic Methylene Blue dye adsorption, Carbohydr. Polym. 147 (2016)
646 79–88. Doi: 10.1016/j.carbpol.2016.03.099
647 [66] A.S. Helal, E. Mazario, A. Mayoral, P. Decorse, R. Losno, C. Lion, S. Ammar, M.
648 Hémadi, Highly efficient and selective extraction of uranium from aqueous solution
649 using a magnetic device: succinyl-β-cyclodextrin-APTES@maghemite nanoparticles,
650 Environ. Sci. Nano. 5 (2018) 158–168. Doi: 10.1039/C7EN00902J
651 [67] F.L. Rivera, F.J. Palomares, P. Herrasti, E. Mazario, Improvement in heavy metal
652 removal from wastewater using an external magnetic inductor, Nanomaterials 9
653 (2019) 1508. Doi: 10.3390/nano9111508
654 [68] Y. Li, A.R. Zimmerman, F. He, J. Chen, L. Han, H. Chen, X. Hu, B. Gao, Solvent-

655 free synthesis of magnetic biochar and activated carbon through ball-mill extrusion
656 with Fe_3O_4 nanoparticles for enhancing adsorption of methylene blue, Sci. Total
657 Environ. 722 (2020) 137972. Doi: 10.1016/j.scitotenv.2020.137972
658 [69] F.L. Rivera, F.J. Recio, F.J. Palomares, J. Sánchez-Marcos, N. Menéndez, E. Mazarío,
659 P. Herrasti, Fenton-like degradation enhancement of methylene blue dye with
660 magnetic heating induction, J. Electroanal. Chem. 879 (2020) 114773. Doi:
661 10.1016/j.jelechem.2020.114773
662 [70] C.-M. Hung, C.-W. Chen, Y.-Z. Jhuang, C.-D. Dong, Fe_3O_4 magnetic nanoparticles:
663 Characterization and performance exemplified by the degradation of Methylene Blue
664 in the presence of persulfate, J. Adv. Oxid. Technol. 19 (2016) 43-51. Doi:
665 10.1515/jaots-2016-0105
666 [71] A. Ghauch, A.M. Tuqan, N. Kibbi, S. Geryes, Methylene blue discoloration by heated
667 persulfate in aqueous solution, Chem. Eng. J. 213 (2012) 259–271. Doi:
668 10.1016/j.cej.2012.09.122

669 **Figure captions**

670 **Fig. 1.** (a) TEM micrograph of Fe_3O_4 NPs synthetized in a 40 mM NaCl solution using an
671 electrochemical flow cell, equipped with iron electrodes, for 1 h at I_{app} = 0.7 A. (b) Room
672 temperature Mössbauer spectrum of the as-synthetized Fe_3O_4 NPs. (c) SEM image of bare
673 RVC substrate (45 ppi). (d) SEM image of Fe_3O_4-modified RVC.

674 **Fig. 2.** (a) Cyclic voltammetry (—) in N_2-saturated medium using a glassy carbon (GC) RDE
675 coated with an ink made of Fe_3O_4 NPs + Vulcan XC-72 carbon black as working electrode,
676 recorded at v = 5 mV s^{-1} without rotation. Linear sweep voltammetries in the same medium,
677 with 2 mM PDS, using the same working electrode (—) or an unmodified GC RDE (- -).
678 Linear sweep voltammetries in O_2-saturated medium, without PDS, using the modified (—)
679 or the unmodified GC RDE (- -) as working electrode. Linear sweep voltammetry in O_2-
680 saturated medium, with 2 mM PDS, using the modified GC RDE (—). All linear sweep
681 voltammograms were recorded at v = 5 mV s^{-1} and ω = 1600 rpm, using a three-electrode
682 cell containing a 0.1 M Na_2SO_4 solution at pH 3.5, with an Ag|AgCl (sat. KCl) and a graphite
683 rod as reference and counter electrodes. (b) Percentage of color removal vs. time during the
684 treatment of 200 mL of solutions containing 50 mg L^{-1} (0.15 mM) MB and 50 mM Na_2SO_4
685 at pH 3.5, at constant I_{app} = 10 mA using an undivided glass reactor equipped with an Fe_3O_4-
686 modified RVC piece and a graphite rod as the cathode and anode, respectively. One trial was
687 made in an N_2-saturated solution in the presence of 1 mM PDS, whereas the other one was
688 made without PDS in an O_2-saturated solution.

689 **Fig. 3.** (a) Effect of I_{app} on the percentage of color removal over time during the treatment of
690 200 mL of N_2-saturated solutions containing 50 mg L^{-1} (0.15 mM) MB and 50 mM Na_2SO_4
691 at pH 3.5 using the same reactor and electrodes described in Fig. 2. (b) Dissolved TOC

692 content at the end of the four trials. The difference between these values and TOC value at 0
693 min (TOC_0) accounts for the organic carbon adsorbed throughout the tests.

694 **Fig. 4.** (a) Effect of PDS concentration on the time course of the percentage of color removal
695 during the treatment of 200 mL of dye solutions analogous to those described in Fig. 3 at I_{app}
696 = 10 mA, using the same reactor and electrodes. (b) Effect of I_{app} under the conditions of plot
697 (a) at 2 mM PDS. (c) Dissolved TOC content at the end of the trials of plot (b), accounting
698 for the percentage of TOC removal depicted on the right y-axis. The difference between these
699 values and TOC_0 corresponds to the organic carbon adsorbed throughout the tests.

700 **Fig. 5.** (a) Time course of the percentage of color removal during the treatment of 200 mL of
701 dye solutions analogous to those described in Fig. 4 at 2 mM PDS and I_{app} = 10 mA, using
702 the same reactor and a freshly prepared Fe_3O_4-modified RVC cathode reused for five
703 consecutive runs (45 min each). (b) Dissolved TOC content (left y-axis) and percentage of
704 TOC removal (right y-axis) at the end of the trials of plot (a). The difference between the
705 former values and TOC_0 corresponds to the organic carbon adsorbed throughout the tests.

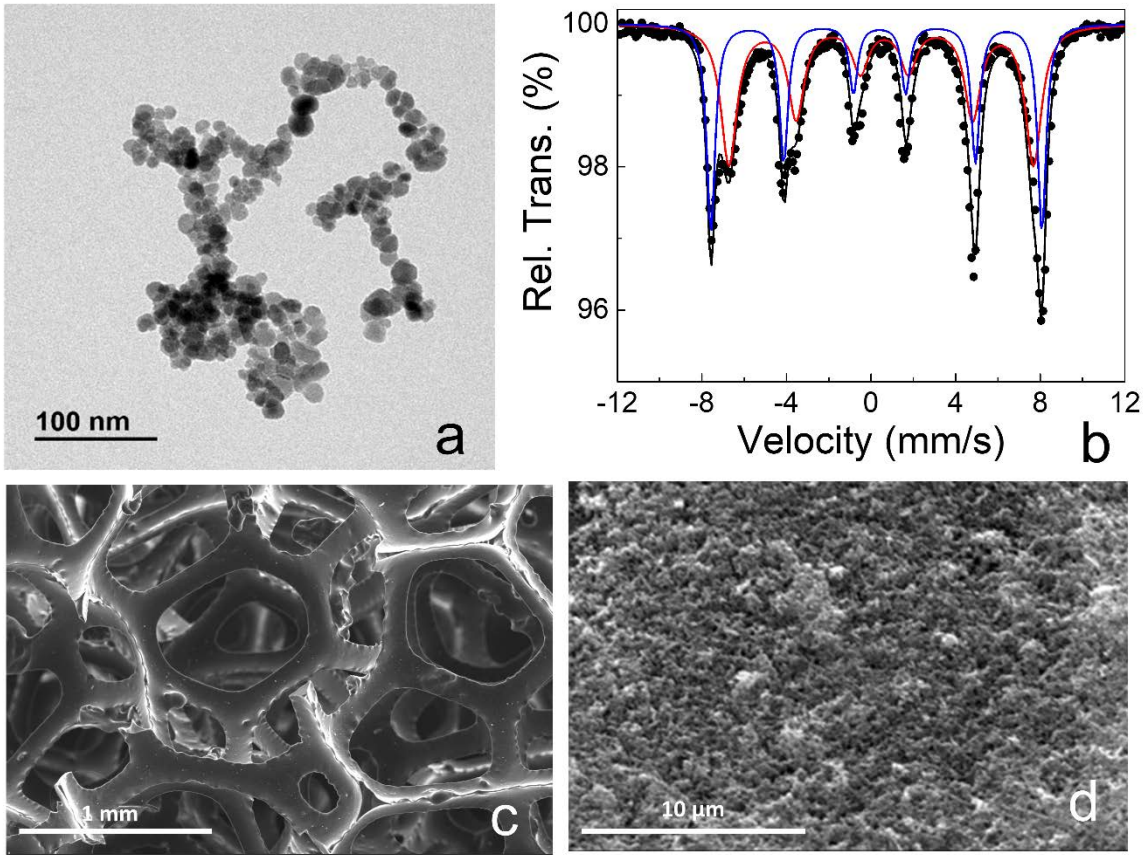
100 nm
a
100
98
96
Rel. Trans. (%)
-12
-8
-4
0
4
8
12
Velocity (mm/s)
b
1 mm
c
10 µm
d

Fig. 1

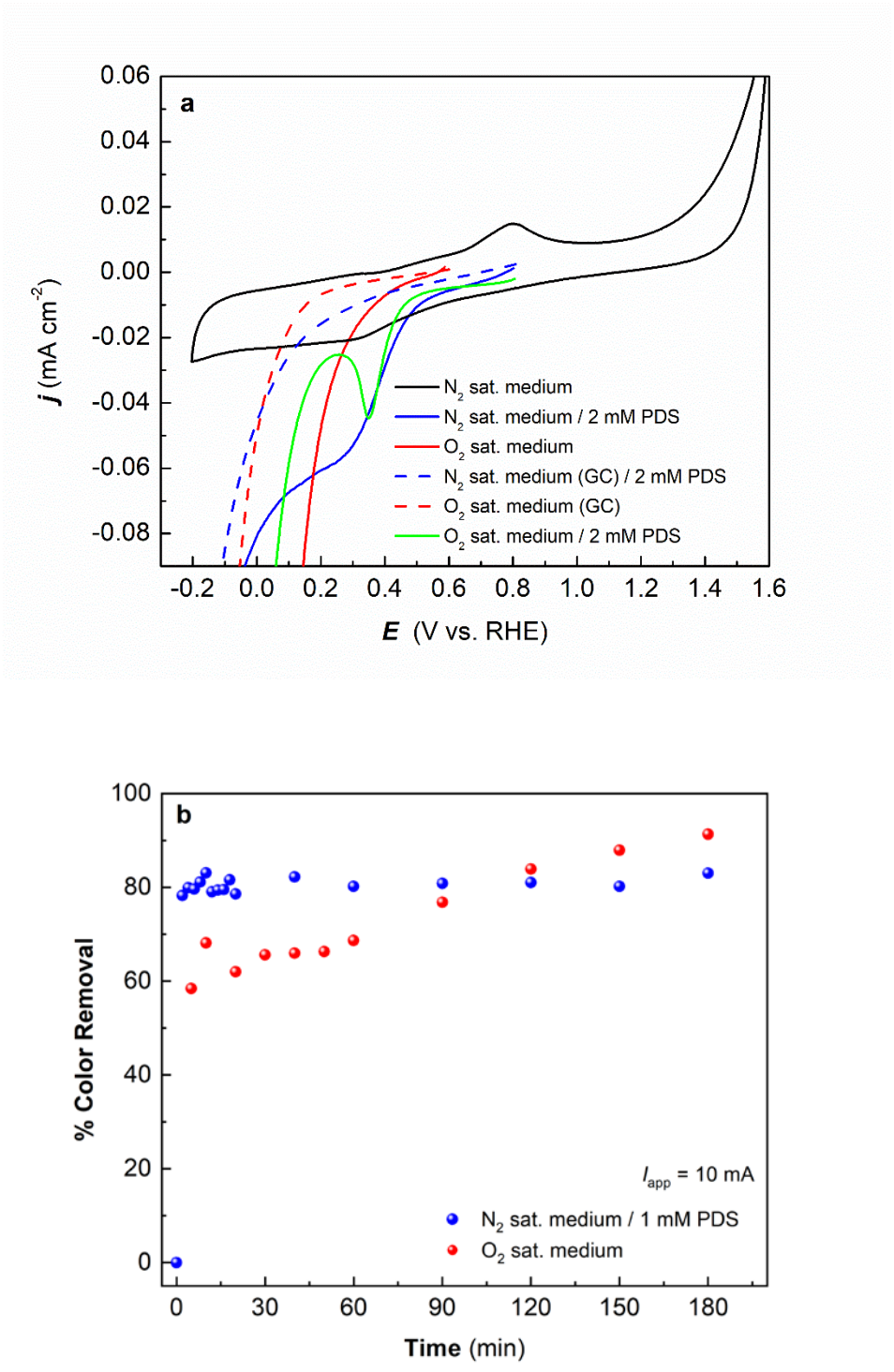
a
0.06
0.04
0.02
0.00
-0.02
-0.04
-0.06
-0.08
j (mA cm-2)
-0.2
0.0
0.2
0.4
0.6
0.8
1.0
1.2
1.4
1.6
E (V vs. RHE)
N2 sat. medium
N2 sat. medium / 2 mM PDS
O2 sat. medium
N2 sat. medium (GC) / 2 mM PDS
O2 sat. medium (GC)
O2 sat. medium / 2 mM PDS
b
100
80
60
40
20
0
% Color Removal
0
30
60
90
120
150
180
Time (min)
Iapp = 10 mA
N2 sat. medium / 1 mM PDS
O2 sat. medium

Fig. 2

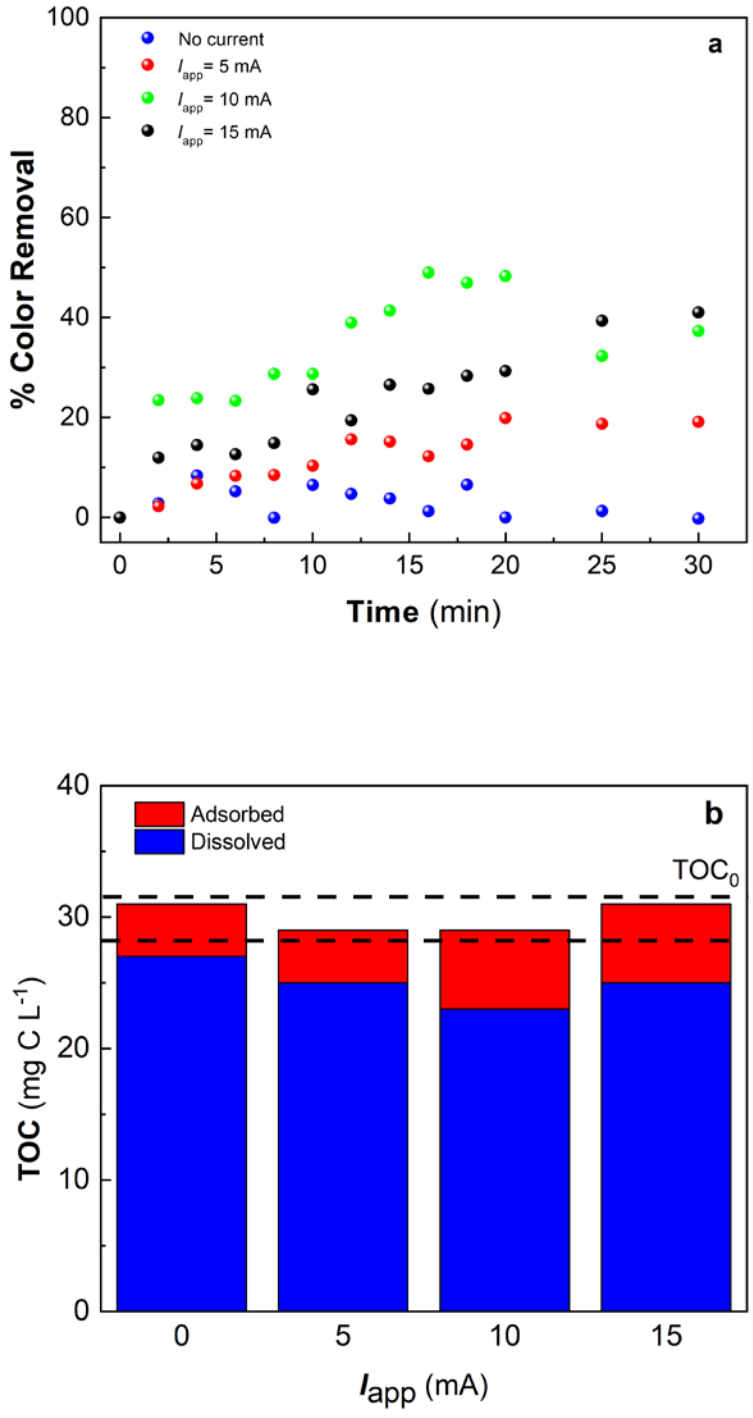
a
No current
I_{app} = 5 mA
I_{app} = 10 mA
I_{app} = 15 mA
% Color Removal
Time (min)
b
Adsorbed
Dissolved
TOC_0
TOC (mg C L^{-1})
I_{app} (mA)

Fig. 3

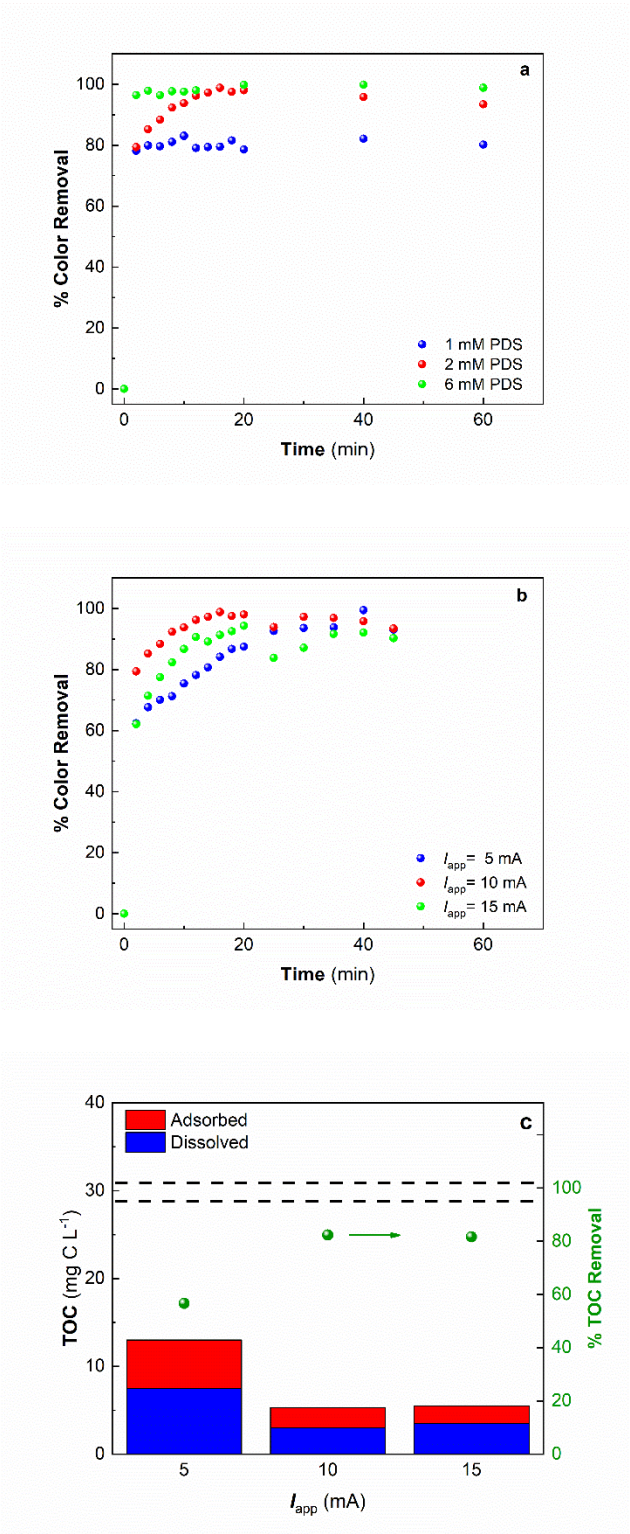
a
% Color Removal
Time (min)
1 mM PDS
2 mM PDS
6 mM PDS
b
% Color Removal
Time (min)
I_{app}= 5 mA
I_{app}= 10 mA
I_{app}= 15 mA
c
Adsorbed
Dissolved
TOC (mg C L^{-1})
% TOC Removal
I_{app} (mA)

Fig. 4

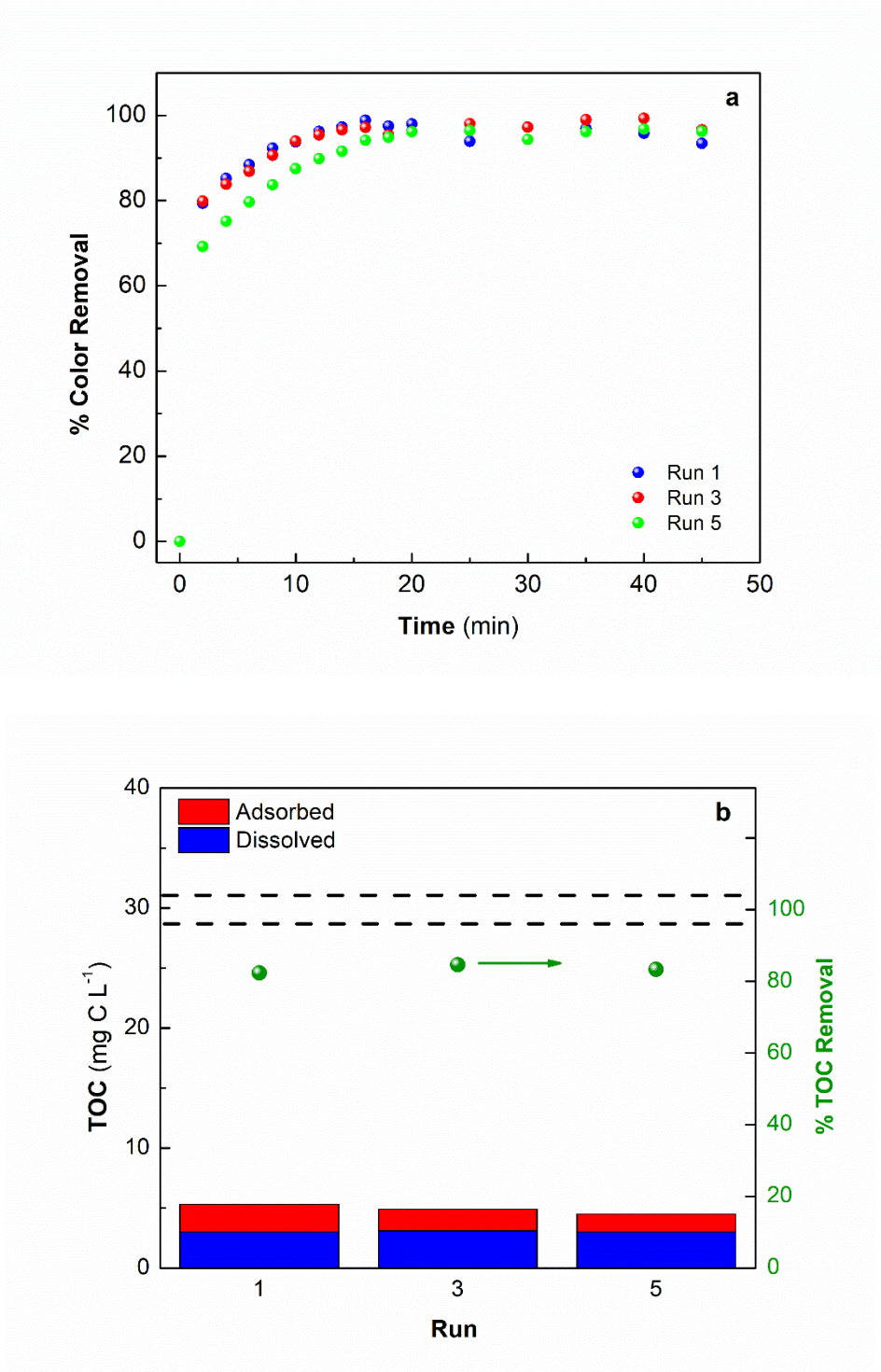
a
% Color Removal
Time (min)
Run 1
Run 3
Run 5
b
Adsorbed
Dissolved
TOC (mg C L-1)
% TOC Removal
Run

Fig. 5